applied sciences

MDPI

Article

Evaluating Collapse Fragility Curves for Existing Buildings Retrofitted Using Seismic Isolation

Amedeo Flora *, Giuseppe Perrone and Donatello Cardone

School of Engineering, University of Basilicata, 85100 Potenza, Italy; giuseppe.perr@alice.it (G.P.); donatello.cardone@unibas.it (D.C.)

* Correspondence: amedeo.flora@unibas.it

Received: 2 April 2020; Accepted: 16 April 2020; Published: 20 April 2020

Abstract: Few studies have investigated so far the collapse capacity of buildings with base-isolation. In such studies, preliminary considerations have been drawn based on a number of assumptions regarding: (i) the methodology used for assessing the collapse capacity, (ii) the collapse conditions and failure modes assumed for both superstructure and isolation system, and (iii) the numerical modeling assumptions. The main results pointed out that the collapse conditions of base-isolated buildings may occur for intensity levels slightly higher than those associated with the design earthquake. In this paper, further developments are made through the use of enhanced models for the description of the behavior of a rubber-based isolation system and the assumption of more rational collapse conditions. Collapse fragility functions, in terms of mean and dispersion values, are proposed for two archetypes representative of existing buildings retrofitted using the seismic isolation technique. The collapse margin ratio (median collapse capacity $S_{a,C}$, namely the spectral acceleration associated to a probability of exceedance equal to 50%, divided by the design spectral acceleration at the collapse prevention limit state) has been evaluated for each examined case-study. Values ranging from 1.10 to 1.45 were found.

Keywords: collapse fragility curves; seismic isolation; non-linear modeling; existing RC-frame buildings

1. Introduction

Collapse fragility functions (CFFs) constitute one of the main components of performance-based earthquake engineering assessment procedures [1,2]. A rigorous approach for the evaluation of CFF is based on non-linear response-time history analysis (NTHA), typically incremental dynamic analysis (IDA) or multiple-stripe dynamic analysis (MSA), performed adopting a specific set of seismic ground motion records, and accurate structural modeling approaches.

The CFF is a cumulative probability distribution (typically in the log-normal form), derived by fitting NTHA (IDA or MSA) results. Basically, CFFs define the structural collapse probability as a function of a reference seismic intensity measure (e.g., the spectral acceleration associated to the fundamental period of the structure, $S_a(T)$). As a matter of fact, CFFs can be identified through a set of two main parameters, i.e., the median "collapse capacity" (i.e., ground motion intensity with 50% probability of exceedance) and the dispersion depending on several uncertainties, including aleatory (record-to-record variability) and epistemic uncertainties (lack of knowledge, design and modeling uncertainties).

In the last decade, several studies aimed at the evaluation of the CFFs for new and existing fixed-base reinforced-concrete buildings [3,4] have been proposed. Conversely, a few studies [5,6] investigated the collapse performances and capacity of existing buildings retrofitted with different isolation systems.

Among those, Cardone et al. [6] proposed CFFs for existing reinforced concrete (RC) framed buildings, located in medium or high-seismicity areas, designed for vertical loads only and equipped with different base-isolation systems.

Recently, the RINTC (Implicit Risk of code-conforming Italian buildings) research project [7], funded within the ReLuis 2015–2018 program (promoted by the Italian Department of Civil Protection), developed a systematic methodology for the estimation of collapse probabilities of different building typologies, included existing buildings retrofitted using seismic isolation. Pragmatic choices regarding the definition of the collapse conditions and the numerical non-linear modeling of the isolation system have been adopted within [7]. The preliminary results of the aforementioned project pointed out that base-isolated systems play a key role in the collapse performances of the whole structure. As a matter of fact, a limited "residual resistance" of the isolation system has been observed after the attainment of the design intensity level, especially for high seismicity areas, in particular for rubber-based systems. Therefore, it can be expected that the definition of the collapse conditions and the numerical non-linear modeling of the rubber-based isolation system can potentially affect the definition of the CFF.

In this paper, the main limitations of the aforementioned work are questioned and further developments of the described methodology, in terms of non-linear modeling and collapse conditions, are proposed for the upcoming version (2019–2021) of the RINTC research project. Such developments are then applied for the estimation of the collapse fragility functions of two archetypes of existing buildings retrofitted with seismic isolation. The CFFs derived from the RINTC research project [7] are finally compared with those obtained adopting the proposed developments. The outcomes of the present study could represent an addendum to the scientific literature providing enhanced tools, potentially suitable for refined performance-based assessment and design procedures.

2. Case Studies

2.1. Superstructure

Two case-studies representative of typical residential RC-frame buildings, located in two different seismicity zones according to the Italian national hazard map, have been examined herein. The relevant seismic parameters of the two sites are listed in Table 1.

Table 1. Seismic parameters of the selected sites.

Case Study	Lat	Long	PGA (T_R = 475y) [g] (Soil Type C)	Seismic Zone
SLD [1]	13.399	42.349	0.345	I
GLD [2]	14.268	40.854	0.24338	II

[1] Seismic Load Design, [2] Gravity Load Design.

The building located in L'Aquila (high seismicity) has been designed with reference to pre-96 seismic regulations (Seismic Load Design—SLD—building) while the one located in Naples (medium seismicity) has been designed for gravity loads only (Gravity Load Design—GLD—building). The superstructure of the selected case-studies features a regular plan of approximately 240 square meters and six above ground-stories. All floor plans are identical, the only differences being restricted to beam-column dimensions and reinforcement. In Figure 1, the typical floor plans of the (a) SLD building and (b) GLD buildings are shown. Shallow beams have been adopted in the internal frames of the aforementioned buildings. It is worth noting that the GLD building (located in Naples) features internal frames only in the Y-direction. All the stories, of both buildings, show the same slab with total thickness (including hollow bricks) equal to 250 mm. The height of the ground level is 3.4 m while that of the remaining stories is equal to 3.05 m. The building structures include the staircase, designed with knee beams. Details about the buildings in the fixed base configuration can be found in [8]. The infills panels are consistent with the traditional practice of the period In particular, a double-layer type with

8 cm (internal layer) and 12 cm (external layer) thick panels constituted by hollow clay bricks and empty cavity (10 cm thick) has been considered.

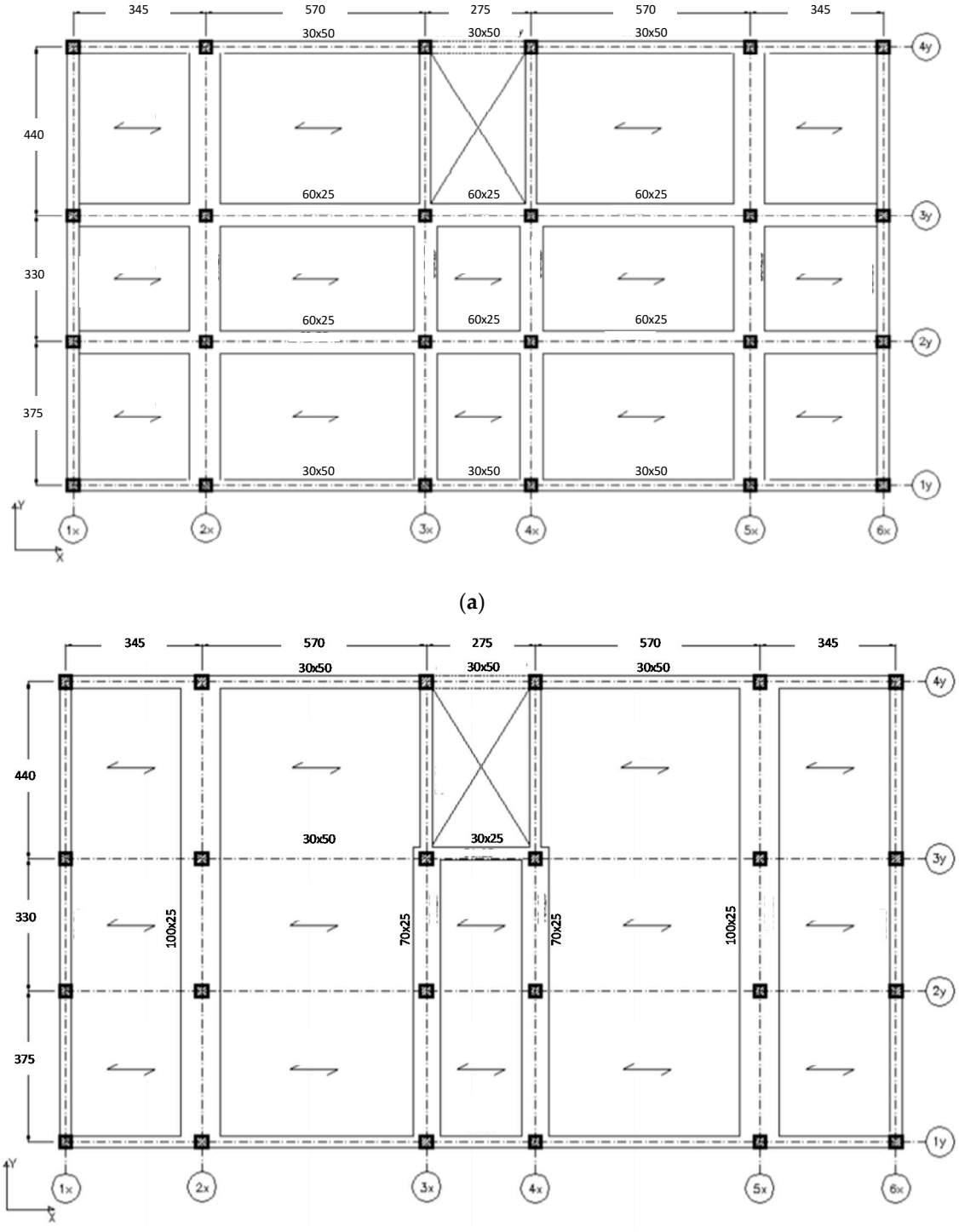

Figure 1. Floor plan with one way slab orientation for (**a**) SLD building and (**b**) GLD building.

2.2. Isolation System

An hybrid isolation system, constituted by high damping rubber bearings (HDRBs, featuring an equivalent damping ratio equal to 0.15 at 100% shear strain), positioned on the building perimeter

and steel-Teflon (PTFE) Flat Sliding Bearings (FSBs, namely, "sliders") positioned below the internal columns of the building (see Figure 2), has been adopted for the retrofit intervention. The described configuration has been selected in order to provide an adequate deformability and, at the same time, a proper torsional stiffness and restoring capability also preventing uplift phenomena in the sliding bearings.

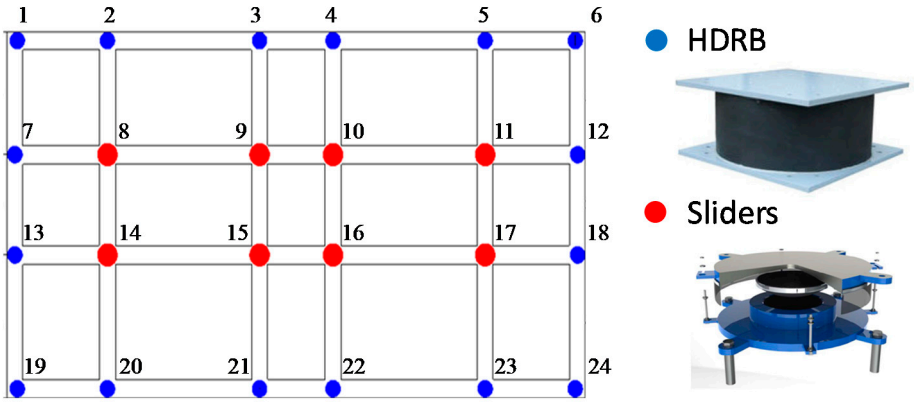

Figure 2. Isolation system configuration.

Modal response spectrum analyses have been performed for the seismic design of the isolation systems. According to the Italian Seismic Code [9], the design objective is represented by the protection of the building's superstructure from any structural damage towards the design earthquake associated with the life-safety limit state (LLS), corresponding to a return period of 475 years. All that considered, the minimum design period of the isolated building ($T_{is,min}$) has been obtained by entering the 15% damped response spectrum using the spectral acceleration target value ($S_d = V_{yield}/M_{total}$) for the superstructure's verification, where V_{yield} is the base shear associated to the first occurring of structural damage in the superstructure while M_{total} represents the total seismic mass of the superstructure.

Table 2 summarizes the main design results. In particular, T_{is} represents the isolation period (including the superstructure deformability), T_{is}/T_{bf} is the isolation ratio between the periods of the isolated and fixed-base configuration (including infill panels), d_{max} is the maximum displacement demand of the bearings. The catalogues of the main Italian manufacturers have been used to select commercial devices, featuring suitable values of effective stiffness and vertical capacity. The main characteristics of the selected catalogue devices, i.e., nominal diameter (ϕ_n) and total rubber height (t_e) for HDRBs; nominal vertical load capacity (V) and displacement capacity (d_c) for sliders, are reported in Table 2.

Table 2. Geometric characteristics and design outcomes for hybrid isolation system.

Case-Study	HDRB ϕ_n/t_e [mm/mm]	Sliders V/d_c [KN/mm]	ξ [%]	d_{max} [mm]		T_{is} [s]	T_{is}/T_{bf} [–]
				HDRB	Sliders		
SLD (L'Aquila)	600/152	3500/600	15	300	300	2.68	3.65
GLD (Naples)	450/102	3500/400	15	200	200	3.3	4.4

The collapse prevention limit state (CPL), associated to a return period equal to 975 years, has then been considered for the verification of the designed system.

3. Numerical Modeling

A non-linear model developed using the OpenSees framework [10] has been adopted for both the isolation system and the superstructure of the case-studies examined herein. Pragmatic choices have been adopted to reduce the computational efforts and the time consumption of each analysis.

3.1. Superstructure

A lumped plasticity model has been implemented for the structural elements (beams and columns) of the examined superstructures. The Ibarra–Medina–Krawinkler [11] model has been assumed to describe the flexural behavior of the plastic hinges. For beams and columns, the skeleton curves of the aforementioned plastic hinges have been derived from moment-curvature analysis of the critical cross sections, considering axial load interaction effects. For the structural members featuring premature shear failure (namely, the short columns of the staircase, identified a-priori), the ultimate rotation capacity has been defined by the intersection between the exhibited flexural behavior and the shear resistance of the specific element [8].

Non-linear elements have been also adopted to model the knee beams of the staircase. Masonry infill panels are modeled with an equivalent compression-only strut. The skeleton curves are derived according to a modified version of the Decanini model [12]. The influence of openings in the infill panels has been considered by a proper reduction of their strength and lateral stiffness. Moreover, potential premature out-of-plane collapse has been also considered. Reference to [8] can be made for all the modeling details.

3.2. Isolation System

As discussed in Section 1, important outcomes regarding the collapse performances of existing buildings retrofitted using seismic isolation have been provided by the ReLuis-DPC 2015-2018 RINTC research project [7]. It is worth noting that, in the aforementioned research project, the High Damping Rubber (HDR) element [13], already included in the Opensees library, has been adopted to describe the cyclic behavior of HDRBs. The latter is a two-node element with 12 degrees-of freedom characterized by easy implementation and computational efficiency. The behavior in the axial direction is able to capture cavitation and post-cavitation phenomena in tension. Moreover, the variability of the critical buckling load and the vertical stiffness with horizontal displacement in compression is taken into account. The model of Grant et al. [14] has been implemented to describe the behavior in the horizontal direction. The coupling effect between axial and horizontal directions is partially considered using mechanical properties in the vertical direction dependent on the shear response parameters. More details about the described model can be found in [15]. However, it is worth noting that, in the model proposed within the RINTC project, response parameters in the horizontal direction are independent of those in the axial direction, neither for large displacements nor for large pressures. Therefore, the axial-shear load interaction (at small and large displacements) as well as P-delta effects due to post-buckling behavior are missed.

All that considered, in the present paper, the mechanical model of the HDRBs has been improved to overcome those limitations. In particular, the Kikuchi bearing element [16] has been adopted in lieu of the HDR bearing model. The Kikuchi bearing element is a two node link element with multi-spring mechanical model which includes two sets of multiple axial springs (one on the top and the other at the bottom of the bearing height) and a set of mid-height multiple (radial) shear springs, all bound together by rigid links. The number of springs can be selected based on the accuracy/convergence of the numerical analysis. The axial behavior of the multiple axial springs (each one representing an individual fiber of the bearing's cross-sectional area) is described by the non-linear AxialSp uniaxial material, available in Opensees. The multiple shear springs system consists of a series of identical springs arranged radially representing the isotropic behavior of the device in the horizontal plane. The non-linear hysteretic behavior of shear springs is represented through the KikuchiAikenHDR material [17]. The buckling behavior associated with high compressive load is simulated by the tilt of the rigid links and interaction between the axial and shear forces of the multiple shear and axial springs. The main advantage of the Kikuchi bearing element is represented by the possibility of capturing the axial-shear load interaction in particular at large displacements. Moreover, the consequent pre- and post- buckling behavior is also taken into account. Figure 3 compares the cyclic responses exhibited by the same elastomeric device (n. 20 of the SLD case-study), modeled using the two

aforementioned elements, subjected to a certain ground motion record (n. 3). As can be seen, while at lower shear deformations the cyclic responses are broadly aligned, in the large deformation range the Kikuchi bearing element shows a reduction of the lateral stiffness at peak horizontal displacement by increasing the amplitude of the applied deformation. This softening response is mainly associated to the axial-shear load interaction, representing a peculiarity of the Kikuchi model.

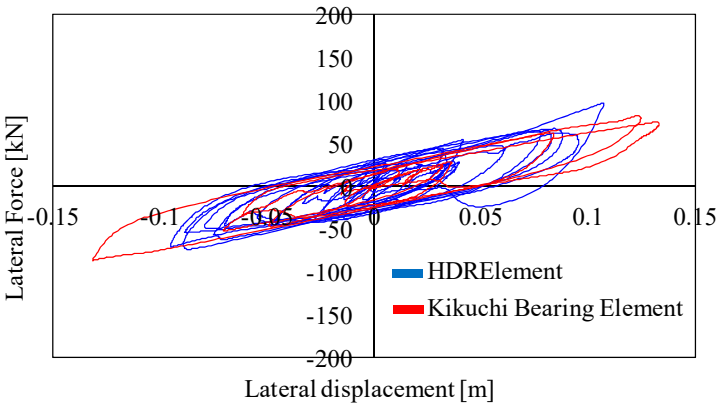

Figure 3. Cyclic response of HDRB n. 20 (SLD case-study) subjected to a certain ground motion record (n. 3), HDR element vs. Kikuchi bearing element.

For the sliders, the same modeling assumptions adopted within the RINTC project have been implemented herein. In particular, a velocity-dependent and axial load-dependent relationship depending on the friction coefficient at low (μ_{slow}) and fast (μ_{fast}) sliding velocities and axial load ratio, has been considered to describe the behavior of the sliders. A value of μ_{fast} = 1% for an axial load ratio equal to 1.0 has been considered. According to Cardone et al. [18], a dynamic-slow friction law 2.5 times lower than the μ_{fast} law has been assumed.

4. Methodology

The seismic performances of the case-study buildings have been evaluated by means of MSA carried out considering 10 intensity levels and 20 ground motions per stripe [7]. A preliminary probabilistic seismic hazard analysis (PSHA) has been carried out using OPENQUAKE [19] to derive the hazard curves at the building sites as a function of the spectral acceleration, $S_a(T)$, associated to the reference period (corresponding to the fundamental period of vibration of the case-study, approximately equal to 3sec in both cases).

Hazard curves are further discretized at the 10 Intensity Measure (IM) values corresponding to the following return periods: 10, 50, 100, 250, 500, 1000, 2500, 5000, 10,000 and 100,000 years.

Then, 20 Seismic records pairs have been selected for each IM based on the proper conditional mean spectra (CMS), assuming an adequate magnitude-distance-deviation disaggregation and a proper attenuation relationship for the selected sites [20].

Assumed that the superstructure and the isolation system can be considered as two components of an in-series system, the collapse of either component induces the collapse of the entire structure.

In line with the mentioned RINTC research project, the collapse of the superstructure has been conventionally associated to the attainment of a top displacement corresponding to a 50% decrease of the lateral strength, computed via pushover analysis in the fixed base configuration [7].

The failure modes considered for HDRBs are cavitation, shear failure and buckling. The same failure criterion adopted in [7] are considered herein for cavitation and shear failure. In particular, cavitation occurs in the post-cavitation branch for an axial tensile strain of the order of 25% while a limit shear strain equal to 350% has been assumed as shear failure deformation threshold.

By contrast, a different failure criterion has been adopted for the buckling mode. In the first edition of RINTC research project [7] (using the HDR element), buckling is deemed to occur when

the P/P_{cr} ratio between the current axial load (P) and the critical buckling load (P_{cr}) is equal to 1, (P_{cr} was computed step by-step as a function of the effective shear rigidity and effective flexural rigidity of the device). The latter criterion underestimates the effective capacity of HDRBs neglecting their post-buckling behavior, thus leading to an excessively conservative collapse condition. As a consequence, in this paper, where HDRBs are modeled with the Kikuchi bearing element (see Section 3), a more "rational" criterion has been assumed considering that the buckling failure is deemed to occur for an axial compressive strain of the order of 50%.

Finally, the failure of FSBs has been associated to the attainment of a certain limit displacement, assumed to be equal to the displacement capacity of the device increased by an extra-displacement equal to a fraction (50%) of the bearing pot radius. In line with the European/Italian seismic Code [9], the connection resistance should be (minimum) two times larger than the maximum shear force value transmitted by the seismic device, as a consequence connections failure has been neglected.

All that considered, the collapse of the isolation system is deemed to occur when at least 50% of the devices reaches one of the failure conditions mentioned above. Failure modes and collapse conditions for the selected case-studies are summarized in Table 3.

Table 3. Failure modes and collapse conditions for base-isolated buildings.

Failure Component	Failure Modes	Collapse Conditions Adopted within RINTC Research Project [7]	Collapse Conditions Adopted in the Present Paper
Superstructure	Ultimate ductility capacity	The relative displacement (difference between top displacement and isolation level displacement) equal to the top displacement derived from Push Over Analisys associated to a peak strength reduction of 50%.	
Isolation System	Buckling	Axial compression force equal or greater than the critical buckling load	Axial compressive deformation equal or greater than 50%
	Cavitation	Occurring of an axial deformation (in tension) εt equal to/larger than 0.25.	
	Shear	Occurring of a shear deformation γ equal to/larger than 3.5	
	Maximum displacement capacity	Occurring of an horizontal displacement equal to/larger than the FPB displacement capacity + half pot device diameter.	

5. Results

In this section the results of the RINTC project [7] have been compared to those obtained adopting the developments proposed in Sections 3 and 4. In this optic, a new set of MSA has been performed implementing the Kikuchi bearing element, in lieu of the HDR element, to describe the behavior of HDRBs. The outcomes of such analysis have been then post-processed considering the failure modes and collapse conditions summarized in the second column of Table 3.

Figures 4a and 5a show the number of collapses and associated failure modes at each IM, for the SLD and GLD case-study buildings, respectively, obtained within the RINTC project [7]. The same results are shown in Figures 6a and 7a with reference to the revised model developed in the present paper. It is worth noting that, in the aforementioned figures, only the first failure occurrence is reported. After that, several other failure conditions can be attained in the same analysis.

Comparing the results of Figure 4a with those of Figure 6a, a slight reduction in terms of number of collapses is observed, for the SLD building, adopting the revised model. In particular, the number of collapses reduces from 3 to 1 at IM6 and from 17 to 14 at IM7, passing from HDR to the Kikuchi bearing element.

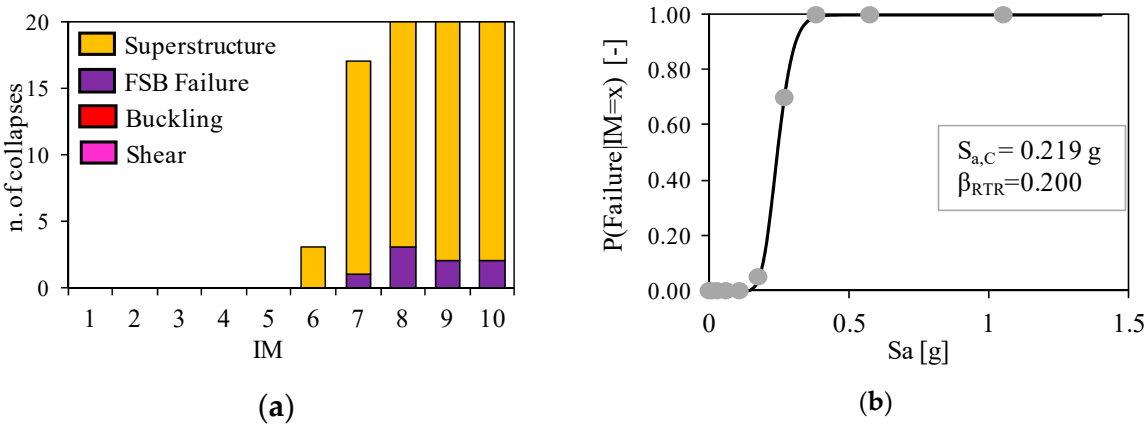

Figure 4. (**a**) Number of collapses for each IM and (**b**) corresponding collapse fragility curve obtained for the SLD case-study within the RINTC research project [7].

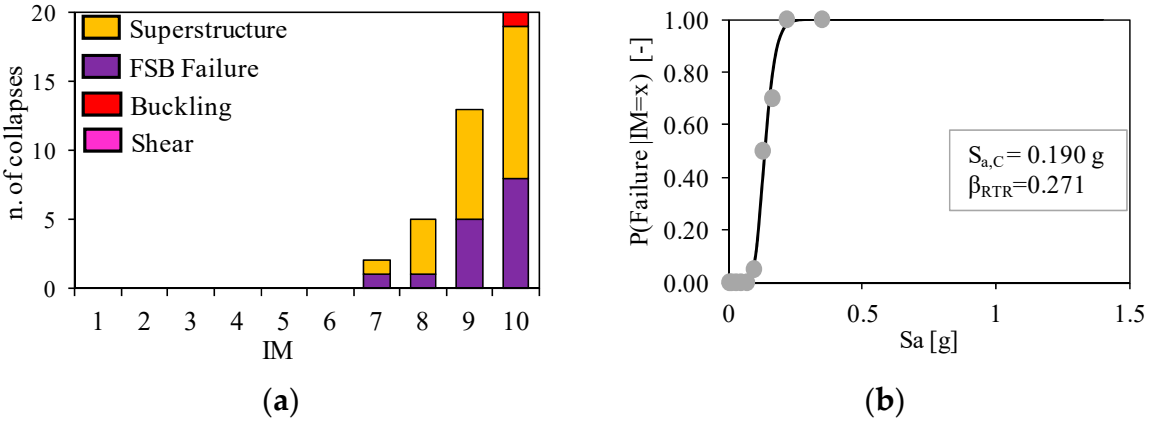

Figure 5. (**a**) Number of collapses for each IM and (**b**) corresponding collapse fragility curve obtained for the GLD case-study within the RINTC research project [7].

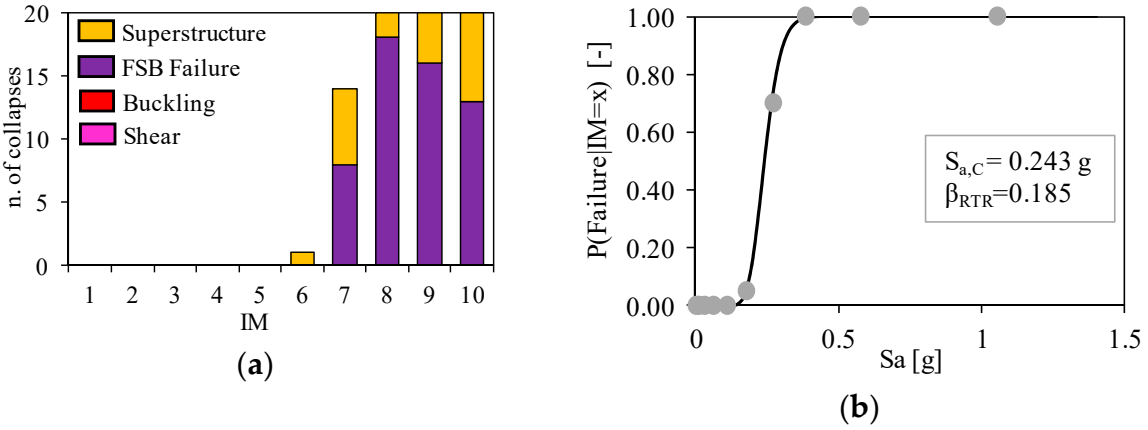

Figure 6. (**a**) Number of collapses for each IM and (**b**) corresponding collapse fragility curve obtained for the SLD case-study adopting the revised model.

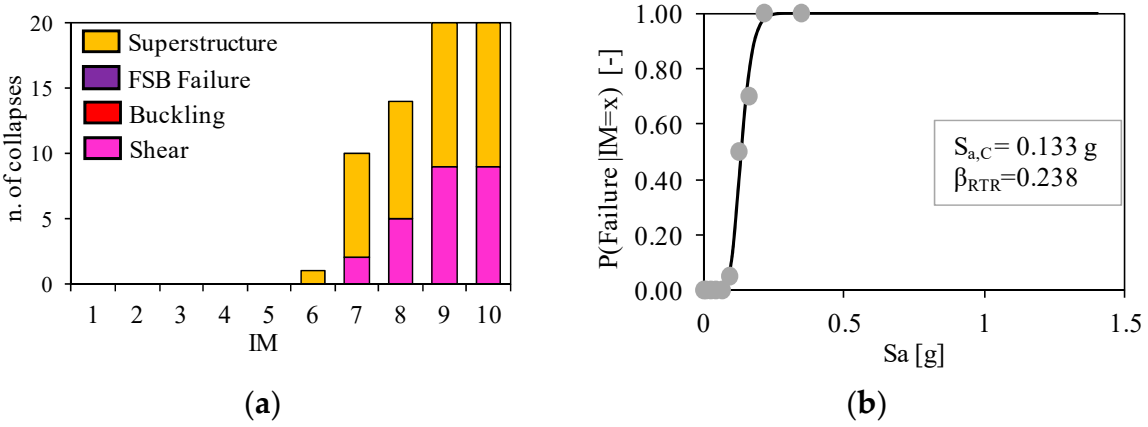

Figure 7. (**a**) Number of collapses for each IM and (**b**) corresponding collapse fragility curve obtained for the GLD case-study adopting the revised model.

On the other hand, a significant reduction of the number of superstructure failures is observed at each IM. This is mainly due to a different seismic response of the isolation system in the two modeling approaches. As a matter of fact, for each ground motion, a larger displacement of the isolation system (Δ_{IS}) is obtained using the Kikuchi bearing element. On the contrary, the corresponding top displacement of the superstructure (Δ_{top}) remains substantially the same. As a consequence, a reduction of the relative displacement ($\Delta_{top} - \Delta_{IS}$) is observed in the revised model (see Figure 8a), thus reducing the probability of collapse of the superstructure. In other words, the horizontal cyclic behavior of the Kikuchi bearing element is characterized by larger displacement demand and lower shear force level towards those exhibited by the HDR element subjected to the same ground motion, especially at large deformations.

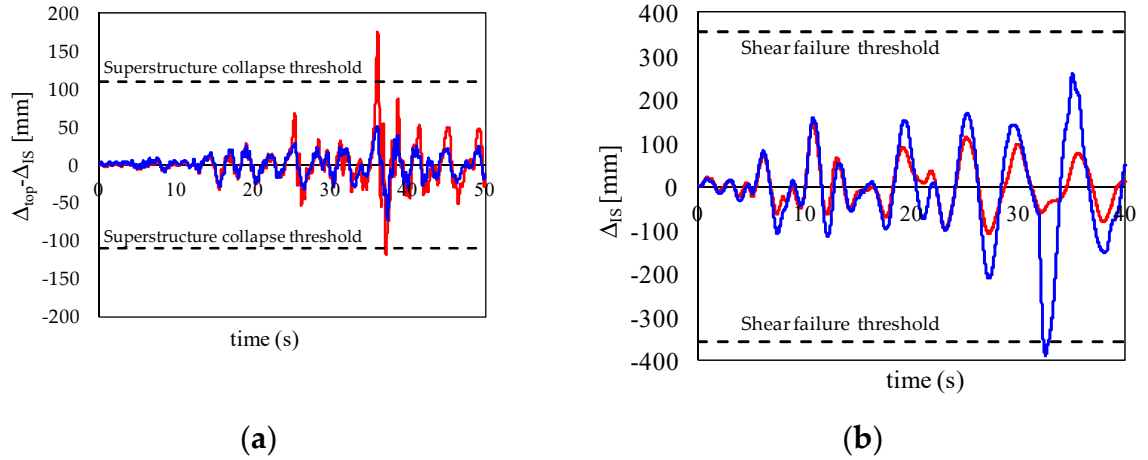

Figure 8. (**a**) Relative displacement vs time for the SLD case-study at IM7—ground motion n. 5 (**b**) Isolation system base displacement vs time for the GLD case-study at IM7—ground motion n. 6.

Figures 4b and 6b show the CFFs for the SLD case-study building derived adopting the two aforementioned modeling approaches. As can be observed, small differences (of the order of 10%) are obtained in terms of median collapse capacity ($S_{a,C}$) and record to record dispersion (β_{RTR}).

A significant increase in terms of number of failures (from 0 to 1 at IM6, from 2 to 10 at IM7, from 5 to 14 at IM8 and from 14 to 20 at IM9) is observed adopting the revised model for the GLD case-study building (see Figures 5a and 7a). As mentioned before, larger displacement demands are obtained adopting the Kikuchi bearing element in lieu of the HDR element. However, in this specific case, the displacement demand level is so larger to produce the attainment of the deformation threshold associated to shear failure for a several number of ground motions (see Figure 8b). The CFFs for the

GLD case-study building, associated to the two different modeling approaches, are shown in Figures 5b and 7b. Significant differences are observed in the GLD case study. In particular, a reduction of approximately 30% is obtained in terms of median collapse capacity, $S_{a,C}$ passing from the RINTC research project modeling approach to the revised model.

Table 4 summarizes the collapse fragility function parameters derived for the case-studies examined and the corresponding values of the collapse margin ratio (CMR, median collapse capacity $S_{a,C}$, divided by the design spectral acceleration at Collapse Prevention limit state).

Table 4. Collapse fragility function parameters and collapse margin ratio (CMR) values derived for the examined case-studies.

Case Study	HDRB Model	Median (g)	Dispersion	CMR
SLD	HDR	0.219	0.200	1.24
	Kikuchi	0.243	0.185	1.37
GLD	HDR	0.190	0.271	2.04
	Kikuchi	0.133	0.238	1.43

Values of CMR larger than 1 have been obtained in each case. Larger values are observed for the GLD case-study building due to a more prudential design of the isolation system.

Finally, record-to-record dispersion values ranging between 0.19 and 0.27 have been obtained. These results are aligned with those proposed by Cardone et al. [6] for similar building typologies.

6. Conclusions

The RINTC (Implicit Risk of code-conforming Italian buildings) research project [7], funded within the ReLuis/DPC 2015–2018 research program, investigated the collapse probabilities of different building typologies, included existing buildings retrofitted using seismic isolation, adopting pragmatic choices regarding the definition of the collapse conditions and the numerical non-linear modeling of the isolation system. In the present paper, developments in terms of non-linear modeling and collapse conditions have been proposed. In particular, an enhanced mechanical model for the description of the behavior of HDRBs is adopted to take into account the axial-shear load interactions (at small and large displacements) as well as P-delta effects due to post buckling behavior. Moreover, a less conservative and more rational criterion has been considered for the estimation of the buckling failure mode of the aforementioned devices.

The revised model has been applied for the estimation of the CFFs of two case-studies representing typical existing buildings retrofitted using seismic isolation, located in two different sites, L'Aquila and Naples (characterized by medium and high seismicity). In particular, the existing building located in L'Aquila (high seismicity) was designed according to the pre-96 seismic code (SLD building) while that located in Naples (medium seismicity) was designed for gravity loads only (GLD building). A hybrid isolation system (HDRBs + FPBs) has been adopted for the retrofit intervention of both case-studies.

For the SLD case-study building, despite a different seismic response of the isolation system is observed passing from the modeling approach adopted within RINTC project to that proposed herein, a limited variation (of the order of 10%) in terms of median collapse capacity ($S_{a,C}$) is obtained. On the other hand, for the GLD case-study building, the implementation of the Kikuchi bearing model and the adoption of a less prudential criterion for the buckling failure lead to more significant effects. As a matter of fact, a sensible reduction in terms of median collapse capacity (of the order of 30%) is observed.

In both cases, slight variations of the record to record dispersion, β_{RTR}, (lower than 10%) are obtained. It is worth noting that the derived dispersion values are in line with those proposed in literature [6].

Generally speaking, the preliminary results presented in this study outline that, in some cases, different choices in terms of failure conditions and modeling assumptions could sensibly affect the

collapse fragility. Further developments are needed to definitively assess the effect of such choices and to identify robust models and rational collapse criteria for each specific case. In this optic, new analysis considering more case-study buildings and isolation system typologies are in progress. In conclusion, the present study represents an improvement of the knowledge geared toward the refinement of the performance-based assessment and design procedures, providing helpful information for specific enhanced modeling assumptions.

Author Contributions: Conceptualization, A.F., G.P. and D.C.; Data curation, G.P.; Formal analysis, A.F.; Investigation, A.F.; Methodology, A.F. and G.P.; Validation, D.C.; Writing—original draft, A.F. and G.P.; Writing—review and editing, A.F. All authors have read and agreed to the published version of the manuscript.

Funding: This research was supported by the Italian Department of Civil Protection.

Acknowledgments: This work has been carried out within the ReLuis RINTC 2019/21 research program. The authors gratefully acknowledge the support of the ReLUIS Consortium for this research. A very special thaks to to Luciano Rocco Salvatore Viggiani for his technical support.

Conflicts of Interest: The authors declare no conflict of interest.

References

1. ATC-Applied Technology Council FEMA P-58. *Next-Generation Seismic Performance Assessment for Buildings*; Federal Emergency Management Agency: Washington, DC, USA, 2012; Volumes 1–2.
2. Cardone, D.; Sullivan, T.J.; Gesualdi, G.; Perrone, G. Simplified estimation of the expected annual loss of reinforced concrete buildings. *Earthq. Eng. Struct. Dyn.* **2017**, *35*, 115. [CrossRef]
3. Haselton, C.B.; Liel, A.; Deierlein, G.G.; Dean, B.S.; Chou, J.H. Seismic Collapse Safety of Reinforced Concrete Buildings. I: Assessment of Ductile Moment Frames. *J. Struct. Eng.* **2011**, *137*, 481–491. [CrossRef]
4. Liel, A.; Haselton, C.B.; Deierlein, G.G. Seismic Collapse Safety of Reinforced Concrete Buildings. II: Comparative Assessment of Nonductile and Ductile Moment Frames. *J. Struct. Eng.* **2011**, *137*, 492–502. [CrossRef]
5. Kitayama, S.; Constantinou, M.C. Collapse performance of seismically isolated buildings designed by the procedures of ASCE/SEI 7. *Eng. Struct.* **2018**, *164*, 243–258. [CrossRef]
6. Cardone, D.; Perrone, G.; Piesco, V. Developing collapse fragility curves for base-isolated buildings. *Earthq. Eng. Struct. Dyn.* **2018**, *48*, 78–102. [CrossRef]
7. RINTC Workgroup. *Results of the 2015–2018 Implicit Seismic Risk of Code-Conforming Structures in Italy (RINTC) Project*; ReLUIS Report; Rete dei Laboratori Universitari di Ingegneria Sismica (ReLUIS): Naples, Italy, 2018.
8. Ricci, P.; Manfredi, V.; Noto, F.; Terrenzi, M.; De Risi, M.T.; Di Domenico, M.; Camata, G.; Franchin, P.; Masi, A.; Mollaioli, F.; et al. Rintc-e: towards seismic risk assessment of existing residential reinforced concrete buildings in Italy. In Proceedings of the 7th ECCOMAS Thematic Conference on Computational Methods in Structural Dynamics and Earthquake Engineering, Crete, Greece, 24–26 June 2019.
9. DM. LL. PP. *17/01/2018: Norme Tecniche per le Costruzioni (NTC2018)*; Gazzetta Ufficiale n. 42 del 20.02.2018: Rome, Italy, 2018. (In Italian)
10. McKenna, F. OpenSees: A Framework for Earthquake Engineering Simulation. *Comput. Sci. Eng.* **2011**, *13*, 58–66. [CrossRef]
11. Ibarra, L.F.; Medina, R.; Krawinkler, H. Hysteretic models that incorporate strength and stiffness deterioration. *Earthq. Eng. Struct. Dyn.* **2005**, *34*, 1489–1511. [CrossRef]
12. Decanini, L.D.; Liberatore, L.; Mollaioli, F. Strength and stiffness reduction factors for infilled frames with openings. *Earthq. Eng. Eng. Vib.* **2014**, *13*, 437–454. [CrossRef]
13. Kumar, M.; Whittaker, A.S.; Constantinou, M.C. An advanced numerical model of elastomeric seismic isolation bearings. *Earthq. Eng. Struct. Dyn.* **2014**, *43*, 1955–1974. [CrossRef]
14. Grant, D.N.; Fenves, G.L.; Whittaker, A.S. Bidirectional Modelling of High-Damping Rubber Bearings. *J. Earthq. Eng.* **2004**, *8*, 161–185. [CrossRef]
15. Ragni, L.; Cardone, D.; Conte, N.; Dall'Asta, A.; Di Cesare, A.; Flora, A.; Leccese, G.; Micozzi, F.; Ponzo, C. Modelling and Seismic Response Analysis of Italian Code-Conforming Base-Isolated Buildings. *J. Earthq. Eng.* **2018**, *22*, 198–230. [CrossRef]
16. Ishii, K.; Kikuchi, M. Improved numerical analysis for ultimate behavior of elastomeric seismic isolation bearings. *Earthq. Eng. Struct. Dyn.* **2018**, *48*, 65–77. [CrossRef]

17. Kikuchi, M.; Aiken, I. An analytical hysteresis model for elastomeric seismic isolation bearings. *Earthq. Eng. Struct. Dyn.* **1997**, *26*, 215–231. [CrossRef]
18. Cardone, D.; Gesualdi, G.; Brancato, P. Restoring capability of friction pendulum seismic isolation systems. *Bull. Earthq. Eng.* **2015**, *13*, 2449–2480. [CrossRef]
19. Pagani, M.; Monelli, D.; Weatherill, G.; Danciu, L.; Crowley, H.; Silva, V.; Henshaw, P.; Butler, L.; Nastasi, M.; Panzeri, L.; et al. OpenQuake Engine: An Open Hazard (and Risk) Software for the Global Earthquake Model. *Seism. Res. Lett.* **2014**, *85*, 692–702. [CrossRef]
20. Iervolino, I.; Spillatura, A.; Bazzurro, P. Seimic structural reliability of code-conforming Italian buildings. *J. Earthq. Eng.* **2018**, *22*, 5–27. [CrossRef]